OPEN ACCESS

University of BRISTOL

Marzo, A., & Drinkwater, B. W. (2019). Holographic acoustic tweezers. *Proceedings of the National Academy of Sciences of the United States of America*, *116*(1), 84-89. https://doi.org/10.1073/pnas.1813047115

Peer reviewed version

Link to published version (if available):
10.1073/pnas.1813047115

Link to publication record in Explore Bristol Research
PDF-document

This is the author accepted manuscript (AAM). The final published version (version of record) is available online via [insert publisher name] at [insert hyperlink] . Please refer to any applicable terms of use of the publisher.

University of Bristol - Explore Bristol Research
General rights

This document is made available in accordance with publisher policies. Please cite only the published version using the reference above. Full terms of use are available:
http://www.bristol.ac.uk/red/research-policy/pure/user-guides/ebr-terms/

Holographic Acoustic Tweezers

Asier Marzo[1], **Bruce Drinkwater**[2]

[1]Universidad Publica De Navarra, [2]University of Bristol

Submitted to Proceedings of the National Academy of Sciences of the United States of America

Acoustic Tweezers use sound radiation forces to manipulate matter without contact. They provide unique characteristics when compared to the more established Optical Tweezers, such as higher trapping forces per unit input power and the ability to manipulate objects from the micrometre to the centimetre scale. They also enable the trapping of a wide range of sample materials in various media. A dramatic advancement in Optical Tweezers was the development of Holographic Optical Tweezers (HOT) which enabled the independent manipulation of multiple particles leading to applications such as the assembly of 3D micro-structures and the probing of soft matter. Now, 20 years after the development of HOT, we present the first realization of Holographic Acoustic Tweezers (HAT). We experimentally demonstrate a 40 kHz airborne HAT system implemented using two 256-emitter phased-arrays and manipulate individually up to 25 millimetric particles simultaneously. We show that the maximum trapping forces are achieved once the emitting array satisfies Nyquist sampling and an emission phase discretisation below π/8 radians. When considered on the scale of a wavelength, HAT provides similar manipulation capabilities as HOT while retaining its unique characteristics. The examples shown here suggest the future use of HAT for novel forms of displays in which the objects are made of physical levitating voxels, assembly processes in the micro-metre and millimetric scale, as well as positioning and orientation of multiple objects which could led to biomedical applications.

Acoustic Tweezers | Contactless manipulation | Acoustic Levitation | Acoustophoresis | Displays

Introduction

In 1986, Ashkin showed that dielectric particles can be trapped in a focused laser beam[1] and that this principle also works for bacteria as well as viruses[2]. Since then, Optical Tweezers have become a fundamental tool in biology and physics, leading to the measurement of the DNA spring constant[2], transport of Bose-Einstein condensates[4,5] and trapping of cold atoms[6]. Holographic Optical Tweezers (HOT)[7,8,9,10] further extended this functionality to enable the simultaneous manipulation of multiple particles resulting in applications such as the assembly of 3D colloidal structures[11], quasicrystals[12,13] and nanowires[14] as well as the probing of soft matter[15].

Acoustic Tweezers use the radiation forces exerted by ultrasonic waves to trap particles[16,17] ranging from less than 1 μm[18,19] to more than 1 cm[20] in various media such as air[20], water[21] and potentially (only proven theoretically) in biological tissue phantoms[22,23]. Acoustic radiation forces are 5 orders of magnitude higher per unit input power than in optical trapping giving them a significant efficiency advantage and enabling low-power operation which is critical in cell manipulation applications[24]. Consequently, Acoustic Tweezers are becoming a fundamental tool for disease diagnosis[25], lab-on-a-chip manipulation[26], centimetre scale containerless processing[27,20] and *in-vivo* applications such as the manipulation of kidney stones[28].

Recent advances have enabled the dynamic positioning of acoustically trapped particles in 1-[27], 2-[20] and 3-dimensions[29,30,31], however, the particles were moved as a group, with no individual particle control. Acoustic radiation force devices using 3D printed lenses have also been used to produce complex patterns of particles[32], but these patterns were static and two-dimensional. Similarly, by multiplexing a focal point it was possible to manipulate in mid-air two droplets of water in 2D[33]. To date, the most versatile dynamic device enables two particles to be manipulated independently in 2D using a ring of emitters in a microfluidic chamber[21].

Being able to individually control many particles with the versatility and efficiency of Acoustic Tweezers would enable many new applications such as display spaces where levitated physical voxels form objects in 3D, or fabrication of structures ranging from the micro-scale for tissue engineering to the centimetre scale for placement of integrated circuits. Also, the inherent capability of ultrasound to act through tissue, would permit the use of HAT for complex *in-vivo* procedures in which trapped particles assume different manipulation roles, e.g. hold, orientate, release, bring together or separate.

In this paper, we explore the capabilities of HAT to dynamically manipulate multiple particles simultaneously in mid-air. We describe and evaluate a novel algorithm that for the first time enable the realization of HAT by controlling the emitted field from ultrasonic phased-arrays. For Optical Tweezers, the Digital Light Modulator (DLM) was revolutionary as it provided more than 500x500 pixels of phase control[7]. Acoustic lenses have recently been exploited to apply similar high-resolution phase modulation[32], but they are static and thus not suitable for dynamic HAT. Phased-arrays are the current dynamic acoustic emitter that offers the best potential solution, e.g. emitters of up to 50x50 elements have been described in the literature[34], however, this acoustic array contains two orders of magnitude less elements than commonly available DLMs. We show that despite this reduced element count, it is possible to realize a HAT with

Significance

Holographic Optical Tweezers use focused light to manipulate multiple objects independently without contact. They are used in tasks such as measuring the spring-constant of DNA, the pulling force of the kinesin protein or to trap matter in exotic states. Differently, Acoustic tweezers use sound radiation forces to trap particles at a larger scale (i.e. from micrometres to centimetres). However, previous implementations did not provide individual control. We present the first realization of Holographic Acoustic Tweezers (HAT). Using an array of sound emitters, we engineer the generated sound field to manipulate multiple particles individually. This enables applications in contactless assembly both at the micrometre and centimetre scale as well as the creation of displays in which the pixels are levitating particles.

Reserved for Publication Footnotes

Submission PDF

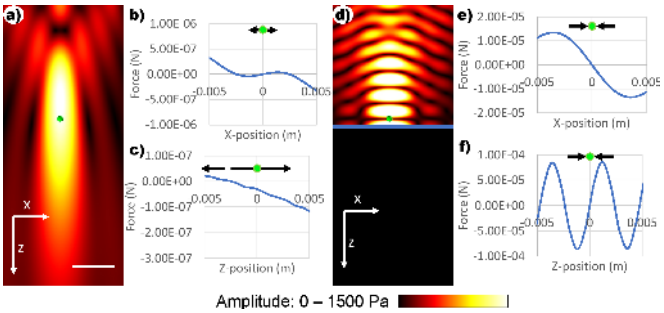

Fig. 1. Trapping over a reflective surface. (a) Pressure amplitude generated by an array focused at a single point in free space, (d) pressure amplitude when the same focal point reflects on a surface (blue line). Trapping forces in the x-direction (b,e) and z-direction (c,f) generated by the focal point. (b,c) Non-converging forces without a reflector, (e,f) converging forces in the presence of a reflector. Scale bar from (a) represents 2cm. Particle is located at the origin.

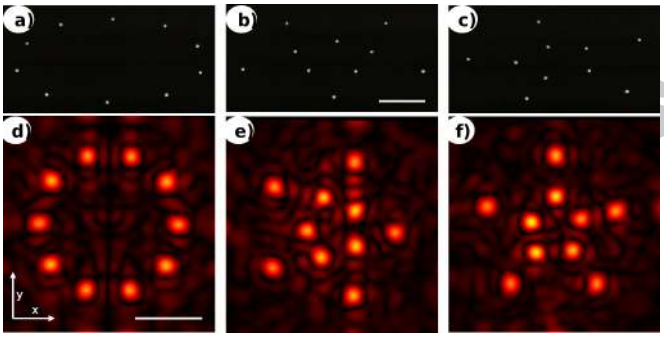

Fig. 2. Simultaneous in-plane manipulation of 10 EPS particles of 2mm diameter. The particles are trapped 2.3mm (λ/4) above a reflective surface. a) the particles start in a circle, b) odd particles move towards the centre, c) the two concentric circles of particles rotate in opposite directions. d,e,f) The simulated pressure amplitude fields generated at the reflective surface. The 16x16 array was placed parallel to the surface 13cm above it. Scale bar (b) and (d) represents 2cm.

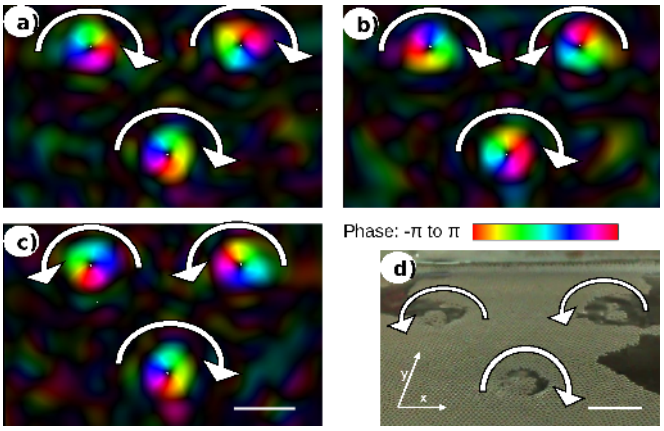

Fig. 3. Generation of vortices with independent chirality. a,b,c) simulated phase profile on a plane parallel to an array placed 15.1 λ (13 cm) above it. a) all the vortices are clockwise. b) The top right vortex has changed to counter-clockwise. c) the top left vortex has also changed to counter-clockwise. d) bubbles on the surface of a water tank rotate according to the direction of the vortices from (c). Scale bar (c) and (d) represents 2cm.

independent manipulation capabilities similar to those achieved in HOT.

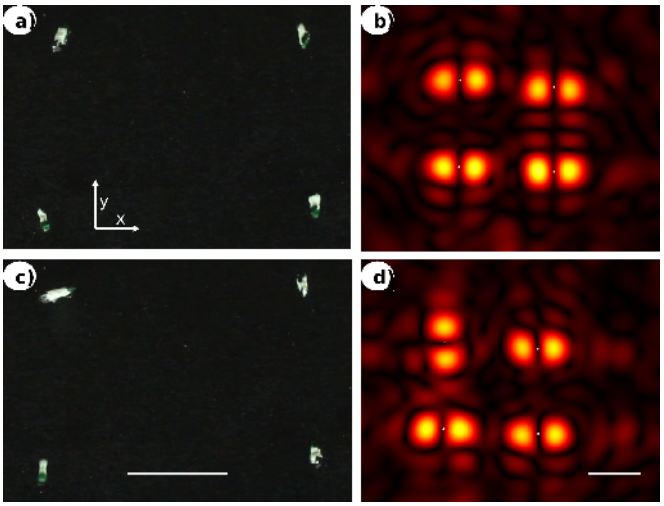

Fig. 4. Individual orientation of asymmetric particles trapped above a reflective surface with an array placed 15.1 λ (13 cm) above it. a) all EPS particles aligned along the y-axis, b) one EPS particle is orientated along the x-axis. b,d) corresponding simulated pressure amplitude at the reflecting surface. Scale bar (c) and (d) represents 2cm.

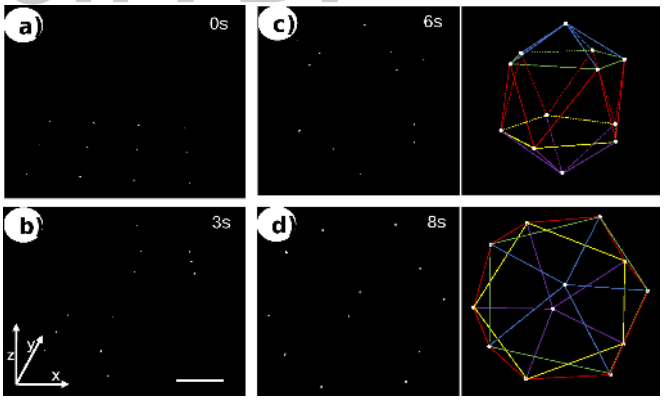

Fig. 5. Simultaneous manipulation of 12 particles starting in a planar grid and being morphed into a 3D icosahedron. a) the particles start in a single plane as a 3x4 grid. b) the particles are moved towards their target z-positions. c) the particles move to form an icosahedron. d) the icosahedron is rotated 45 degrees towards the viewer. For (c) and (d) the vertices of the icosahedron have been overlaid. Scale bar (b) represents 2cm.

An algorithm capable of realizing HAT is distinctly different from those used previously for HOT. In optics, a focus on the particle is sufficient for trapping[35] whereas in acoustics, only negative contrast particles (i.e. the acoustic impedance of the particle is less than that of the medium) will be trapped in this way[36]. However, acoustic trapping in air and most particles in water-based media lead to positive acoustic contrast particles. Therefore, in practice, acoustic trapping is only achieved at the zero pressure regions of standing-waves nodes[27], focused vortices[37], twin-traps[30] or bottle-beams[30].

Here, we describe a novel Iterative Backpropagation (IB) algorithm that we use to calculate the emission phases of the array elements to realise a functional HAT. This algorithm uses a modified version of the Iterative Angular Spectrum Approach[32] (IASA), IASA is itself based on the Gerchberg-Saxton (GS) algorithm[38]. Differently from IASA and GS, IB uses propagators derived from a specific transducer model which enables us to accurately predict the acoustic field with minimum computational effort. In addition, IB permits the creation of focal points as well

sion PDF

as the enforcement of phase dependencies between these points allowing us to efficiently generate different traps (i.e. focal points, twin-traps and vortices) at arbitrary positions.

We show that HAT can be realised using this algorithm and two 256-emitter arrays with an element spacing and diameter of 1.2λ (1cm) operating at 40 kHz with a phase resolution of π/16 radians and an update rate of 90 frames per second. For in-plane 2D manipulation we used a single array placed 15.1λ (13cm) above a sound-reflective surface, for 3D manipulation we used two opposed arrays separated by 26.7λ (23cm) (Figure S1), these separations were selected to provide high acoustic pressure in the desired planar or volumetric manipulation region (Figure S2). We use these systems to demonstrate the controlled manipulation of multiple Expanded Polystyrene (EPS) spheres (1-3mm diameter) (Movie S1).

Results

In-plane manipulation

The multi-particle manipulation capabilities of HOTs are usually demonstrated with the control of various particles in a single plane[7]. Here, we realize an in-plane HAT with the particles initially resting on a reflective surface. This is a common practical scenario, e.g. with particles resting on a microscope cover slide[39]. If a sound beam is focused on a particle situated on a reflective surface, due to the interference between the incoming and reflected field, a local standing wave is created with the first node positioned λ/4 above the surface (Figure 1). At this node, the forces in all three dimensions converge, which is the requirement for stable trapping. Thus, for particles located on a planar reflective surface, HAT can be realized by focusing the array on the particles and manipulating these foci.

Multiple particles are manipulated by generating multiple foci, causing the particles to be trapped in the nodes formed just above the reflector. The IB algorithm (see Methods) is used to generate focal points at the positions of the particles and the emitter phases are dynamically controlled to move the foci and hence the particles. The application of the IB algorithm ensures that the pressure amplitudes at the foci are maximized and that the deviation between the various points is minimized, i.e. the normalized standard deviation of the focal pressure amplitude is reduced by 30% when compared with the non-iterative method (see Methods). In Figure 2 and Movie S2, we show the manipulation of 10 particles in a plane λ/4 above a reflector.

The minimum distance achieved between the particles was ≈1.3 cm (1.5λ) regardless of the number of trapping points (Figure S3). At smaller distances, the focal points merged together inhibiting independent control. The Rayleigh resolution limit[40] for this configuration is 0.85cm ($1.22\lambda L/A$ where $L=13$cm is the focal distance and $A=16$cm is the aperture), but this minimum distance between traps can only be obtained with s smaller acoustic emitters, we show the amplitude distribution of two close focal points depends on the pitch of the array in Figure S4.

Here, at excitation signals of 10Vpp (9.5W of input power), we manipulated 12 particles (Figure 2); and at 16Vpp with double the number transducers (57W of input power), we manipulated 25 particles (Movie S3). In Figure S5, we show that when attempting to use our system to generate 28 traps, the generated undesired artefacts (secondary high-amplitude regions that were not defined as focal points) start to become as powerful as the traps. Therefore, for this system, further increase of the power will have no further benefit in terms of the number of independent traps. The effect of artefacts is explored in more detail in the discussion.

Beyond trapping: in-plane torque and orientation

HOT have been used to create traps with different functionalities[7], for example vortices that can transfer orbital angular momentum (OAM). In acoustics, single vortex beams have also been used to trap and transfer OAM[41,42,43,44]. In HAT, we can generate multiple vortices with independent chirality using the IB algorithm, but this time tuned to create vortices. In Figure 3 and Movie S4, we generate 3 vortices above a water surface and individually change their chirality in real time. The vortices were separated by 10λ to correctly observe the rotation of soap bubbles on the surface of the water. With our system, it was possible to bring two vortices cores within ≈1.4cm (1.6λ) (Figure S6) and generate up to 5 discernible vortices (Figure S7).

In the past, it has been shown that an acoustic twin-trap can orientate asymmetric particles[45,30]. The IB algorithm presented in this paper (see Methods) is capable of generating for the first time multiple twin-traps at arbitrary positions and with different orientations. Twin-traps and vortices can create converging forces along the direction of propagation (i.e. z-axis); however, this force was not enough to levitate the particles since it can be more than 30 times weaker than the lateral forces[46]. Hence, we adopted a time-multiplexing approach between twin-traps (to orientate) and focal points (to generate enough trapping force), this approach has been recently demonstrated for one particle[47] but here we show that it can be applied for multiple particles to achieve independent control of particle orientation. In Figure 4 and Movie S5, we show the orientation of 4 asymmetric particles and change their orientations individually by rotation of the twin-traps. With our current configuration, it was possible to generate up to 7 twin-traps (Figure S8) with a minimum distance of ≈1.4λ between them (Figure S9).

3D Manipulation

To realize a 3D HAT we used a double-sided arrangement made of two opposed arrays (16x16 elements) separated by 26.7λ (23cm) to create multiple standing waves with nodes located at the target trapping positions. To do so, the IB algorithm first creates high intensity foci at the specified trapping positions. These foci are then all shifted vertically (in the z-direction) by λ/2 by the application of an additional phase delay of π radians to the top array elements, thereby nodes now occur at the required trapping locations. Hence, the converging forces required for trapping are created and can be manipulated by dynamically moving the foci. In Figure 5 and Movie S6 we show 12 particles that start in a single plane, then morph into an icosahedron that afterwards rotates around different axes. In Holographic Optical Tweezers, this same manipulation has been shown[49], albeit on a much smaller length scale.

In Figure S10 and 11, we use acoustic field simulations to show that the trapping forces decrease linearly with the number of trapped particles. More importantly, keeping the acoustic power per unit area constant and reducing the pitch of the emitters improves the performance of HAT in terms of trapping stiffness. However, we show that, once Nyquist sampling[50] is achieved (emitter pitch of λ/2), no further improvements can be obtained. The HAT presented in this paper has a transducer spacing of 1.2λ and so is somewhat sub-optimal in this regard. We also use acoustic field simulations to show that trapping strength does not increase significantly for phase discretisation levels below π/8 radians (Figure S12). Since our system discretises phase at π/16 radians it is already optimal in that sense. We note that this is consistent with findings from single-trap systems where a phase discretisation of π/5 was found to be sufficient[51].

Up to 27 particles have been manipulated in 3D using holographic optical tweezers[11]. Despite our limited array size (i.e. 16x16 cm), spatial discretisation (i.e. 16x16 elements) and pressure levels (i.e. 15Vpp to generate 2.3 Pa at 1 meter with each emitter), we achieved simultaneous dynamic manipulation of 12 particles (Figure 5) and the partial manipulation of 25 particles (Movie S3). In the last case, some particles escaped the traps as they were being moved due to the increased trapping stiffness required to counteract the oscillations of the particles in air.

Submission PDF

Therefore, reaching the same number of particles as HOT would be feasible employing more powerful or smaller elements.

Discussion

We quantified the quality of the traps using the stiffness (i.e. the spatial gradient of the force), which represents the converging forces of the traps. From our simulations (Figure S10) and experiments (Figure S13) we observed that the trapping forces are inversely proportional to the number of traps created. Simulations show that the stiffness can be improved by decreasing the pitch of the emitters (Figure S10) or by increasing the emission phase resolution (Figure S12). However, when close-packed emitting elements reach a pitch smaller than $\lambda/2$ and an emission phase resolution below $\pi/8$ no further improvement can be obtained.

The IB algorithm maximises the trap quality (i.e. stiffness), rather than minimising artefacts. As a result, artefacts are often present (e.g. Figure 4.b & d, Figure S3 and S5). In general, for a low number of traps (i.e. <10) the traps have significantly larger pressure amplitude than these artefacts and thus more trapping force, so they do not cause a significant problem. However, as the number of traps increases, their trapping forces decrease, and the artefacts become increasingly powerful, this is shown qualitatively in Figure S5 and quantitatively in Figure S14. We note that with the future possibility of ultrasonic arrays with more transducers and a smaller pitch it may be possible to develop algorithms that maximize traps stiffness and also minimise artefacts.

The appearance of artefacts and ghost traps is a very pressing problem in HOT[52], this problem also appears in our HAT system. On the one hand, secondary nodes appear along the Z-axis. The focal points are inherently elongated along the propagation direction (i.e. in an ellipsoidal shape) and this creates multiple secondary nodes separated by $\lambda/2$. The length of the focal zone (or Rayleigh length) depends on the wavelength, aperture of the array and distance from the array. In Figure S15, we show the amplitude profile of focal zones for our system depending on the number of transducers and traps, the Rayleigh length is similar for all cases (i.e. 7 cm ≈ 8 nodes). We note that stronger focusing (i.e. lower F#) can be used to reduce the length of the focal zone and thus reduce the number of secondary nodes.

Undesired secondary traps can also be created in the XY plane, for example a focus at a single point can create secondary areas of high-intensity outside of the focal area following an Airy amplitude distribution[53]. When our phased-array generates multiple focal points, it produces several of these secondary focal points (also called artefacts or ghost traps). In Figure S14 we show how the ratio between the minimum amplitude of the focal points and the maximum amplitude of the artefacts varies with the number of traps. As mentioned before, the traps are significantly stronger than the artefacts for relatively small numbers of traps (i.e. <10) but as the number of traps increase their strength reduces, until they approach that of the artefacts. For the 16x16 element array used here, the ratio is 16:1 for one focal point and decreases to 3:1 for 25 traps. Surprisingly, emitters with finer pitch lead to stronger artefacts (Figure S16.a & b) but have the advantage of generating the secondary lobes further away from the central region (Figure S16.c & d).

A trapped particle will scatter sound and affect nearby particles. However, for the particles used here (i.e. 1-2mm diameter) this effect was small. Supplementary Video 7 shows that particles of 1-2mm diameter do not affect the particles in the nodes above or below in a perceivable way. In Figure S17 we show a simulation of how particles of different diameters affect the nearby acoustic field, e.g. nodes are only displaced by 0.12mm when a 1mm diameter particle is added in the next node, this distortion becomes more pronounced as the particle size increases.

The Rayleigh criterion[40] determines how close 2 focal points can be generated without getting too distorted (e.g. start to merge), hence we considered it to be an adequate indicator of the minimum lateral distance between the traps. In our setup, this minimum distance between traps was 1.4λ which is several times larger than the particle size.

The repositioning accuracy of the particles was ± 0.1mm ($\lambda/86$) for the in-plane and ±0.5mm ($\lambda/17$) for the 3D manipulation. Similar levels (relative to the wavelength) of positional deviations occur in optical trapping, where the particle centre is not always at a constant distance to centre of the focus[7]. The trapped particles showed good stability over time, in Movie S8 a time lapse of 1 hour showed no noticeable deviation apart from that induced from air currents.

Optically trapped particles are often used as handles to manipulate other samples (such as DNA strands[2]). Similarly, we attached EPS spheres to different objects and manipulate these handles, e.g. to post a thread through a hole in a of piece fabric (Movie S1).

The demonstrated system operates in air with a wavelength of 8.6mm but, in principle, HAT can be scaled down by increasing the frequency and applied to other propagation media. For instance, a system operating at 7.5MHz in water-based solutions would have a wavelength of 200um, enabling the trapping of 20um cells (the current HAT can trap particles smaller than $\lambda/10$). The demonstrated 3D HAT employed two arrays of 256 elements, with future systems containing more and smaller elements, or higher emitter output pressure, improved capabilities can be expected. In the medical domain, arrays with twice the number of elements are already available[54]. Similarly, Capacitive Micromachined Ultrasonic Transducers (CMUT) will enable the miniaturization of the systems for working at the microscale wavelength[55].

Larger systems would enable the trapping of more particles and thus allowing the creation of displays made of levitated physical voxels, these displays would have characteristics that no existing display provides. Holograms can only be viewed from specific angles and both volumetric displays or the recent photophoretic displays are based on light reflection, so they can only operate under specific lightning conditions[56].

In the supplementary methods section we describe the manual and semiautomatic approaches employed to load the particles into the system. We note that a combination of HAT with tracking methods would enable an automatic solution for inserting the particles. For example, a 3D tracking system could detect the position of the particles so that the traps are directly created at those positions.

We have presented the first demonstration of Holographic Acoustic Tweezers (HAT) that enables the individual positioning of multiple particles in 2D and 3D. These results have come 20 years after the appearance of its optical analogue (i.e. HOT). The iterative backpropagation (IB) algorithm was the key that unlocked the realization of HAT and hence it is the most novel aspect. It allowed us to create multiple functional traps using arbitrary arrangements of transducers. HAT enables the control of multiple particles individually with the unique advantages of acoustic radiation forces, i.e. scales from micro- to centimeters, support of multiple materials for samples and propagation media and high ratio of input-power to forces.

Materials and Methods

Hardware

We employed arrays of 16x16 1cm diameter 40 kHz ultrasonic transducers (Murata MA40S4S) operating in air. An FPGA (Altera Cyclone IV EP4CE6) receives the phases to be emitted from the computer using UART protocol operating at 250kbauds. Mosfet Drivers (Microchip MIC4127) amplify the signals up to 15Vpp half-square waves, that are fed into the transducers. Due to the narrowband nature of the transducers the output pressure was sinusoidal[51]. This hardware had a phase emission resolution of $\pi/16$ radians and updated 90 times per second. The employed particles were Expanded Polystyrene (EPS) spheres of 1-3 mm diameter.

Algorithm for the HAT Calculation: Iterative Backpropagation (IB)

submission PDF

To generate multiple traps, we employed Iterative Backpropagation (IB), which is a modification of the iterative IASA[32] and GS[38] algorithms. If we have $n$target traps at positions $\boldsymbol{t_1}, \ldots, \boldsymbol{t_n}$ we will split them into multiple control points depending on the desired type of trap. All the resulting control points $\boldsymbol{c_1}, \ldots, \boldsymbol{c_k}$ will have positions $\boldsymbol{t_j}$, amplitudes $a_j$and phases φ_j where j is between 1 and k. Amplitude and phase are represented as a single complex number c_j. The position, amplitude and phase of the control points depends on the type of trap to be generated and are described in the next paragraph. The amplitude associated with a given control point is $n_j = 1/m$ where m is the number of control points use to define a given trap. The phase of the control points starts at 0 radians but it is updated with every iteration of the algorithm. Only the phase of the first control point of a trap (φ_j)is updated; the rest of the points have a fixed phase relative to this first point and this phase pattern depends on the type of trap.

The shape of the three pressure field shapes used to create the traps (i.e. focus, vertical twin-trap and vortex) were found to be almost invariant spatially within the manipulation regions (Figure S18) This allowed us to identify a small number of features (or control points) that characterised each of these trap geometries. A focal point requires a single control point with the same position as the focus and unity amplitude. A twin-trap has control points with a separation of 1.4λ between them, the control points can be rotated around the centre of the trap to control its orientation. A vortex trap is decomposed into 8 control points with the phase pattern following an increase from 0 to 2π radians in the counter-clockwise or clockwise direction depending on the desired chirality of the vortex, the distance between these points and the centre of the trap is 1.4λ. The location and phases of control points in various traps can be seen in Figure S19.

Consider a transducer l emitting with an amplitude a_l and phase φ_l (i.e. $p_l = a_l e^{i\varphi_l}$), to produce a complex field at $\boldsymbol{r}$ given by $p_{l\boldsymbol{r}} = p_l h_{l\boldsymbol{r}}$ where $h_{l\boldsymbol{r}}$ is the complex propagator from the position of transducer l to the point $\boldsymbol{r}$, we pre-calculate the propagators from each transducer to each control point h_{lj}.We obtain this propagator using the far field piston source model and setting the initial phase of the transducer to 0 (see Supplementary Methods). The algorithm then proceeds by iteratively finding the phases for the transducers required to generate the target fields at the control points. If the phases between successive iterations are below a certain threshold (0.01 radians in our case) the algorithm stops, for the examples presented in the paper convergence was achieved after 200 iterations.

1. Forward propagate the transducer's complex pressure to the control points. $c_j = \sum p_l h_{lj}$

2. Normalize the amplitude at the control points and set the phase. $c_j = n_j c_j / |c_j|$ where n_j is the relative amplitude for the point j. For all the points m which are not the first point of the trap, the phase is set in relation to the first point.

3. Time reverse the control points into the transducers. $p_l = \sum c_j \overline{h_{lj}}$. Where $\overline{h_{lj}}$ is the conjugate of the complex propagator.

4. Normalize the output amplitude of the transducers. $p_l = p_l / |p_l|$

This algorithm supports the generation of focal points, twin-traps and vortices at the target positions. Furthermore, the angle of the twin-trap or the direction of the vortex is tunable by the user via the definition of the control points.

Using the above IB algorithm alone was sufficient for in-plane manipulations. However, for generating the nodes required for 3D manipulation, an additional step was used. First, as with 2D trapping, the IB algorithm is used to generate focal points at the trapping positions. Second, a π radians offset is added to all elements in the top array to shift the high intensity focus (i.e. an antinode) so that nodes are located at the target positions (Figure S20).

Using a direct time reversal method (i.e. IB with 1 iteration) provided similar results in terms of mean force magnitudes (Figure S21) but the variation between traps was larger (Figure S22). A brute-force global maximization of the Gor'kov Laplacian (trapping stiffness) for all the traps as an extension to Marzo et al. algorithm[30] did not produced functional traps.

Submission PDF

Acknowledgements

This project has been funded by the UK Engineering and Physical Science Research Council (No. EP/N014197/1).

1. Ashkin A, Dziedzic JM, Bjorkholm JE, Chu S (1986) Observation of a single-beam gradient force optical trap for dielectric particles. Optics letters **11**(5), 288-290.
2. Ashkin A, Dziedzic JM (1987) Optical trapping and manipulation of viruses and bacteria. Science **235**(4795), 1517-1520.
3. Wang MD, Yin H, Landick R, Gelles J, Block, SM (1997) Stretching DNA with optical tweezers. Biophysical journal **72**(3), 1335-1346.
4. Gustavson TL, Chikkatur AP, Leanhardt AE, Görlitz A, Gupta S, Pritchard DE, Ketterle W (2001) Transport of Bose-Einstein condensates with optical tweezers. Physical Review Letters **88**(2), 020401.
5. Kozuma M, Deng L, Hagley EW, Wen J, Lutwak R, Helmerson K, ..., Phillips WD (1999) Coherent splitting of Bose-Einstein condensed atoms with optically induced Bragg diffraction. Physical Review Letters **82**(5), 871.
6. Ketterle W, Davis KB, Joffe MA, Martin A, Pritchard DE (1993) High densities of cold atoms in a dark spontaneous-force optical trap. Physical review letters **70**(15), 2253.
7. Curtis JE, Koss BA, Grier DG (2002) Dynamic holographic optical tweezers. Optics communications **207**(1-6), 169-175.
8. Dholakia K, MacDonald M, Spalding G (2002) Optical tweezers: the next generation. Physics world **15**(10), 31.
9. Molloy JE, Padgett MJ (2002) Lights, action: optical tweezers. Contemporary physics **43**(4), 241-258.
10. McGloin D (2006) Optical tweezers: 20 years on. Philosophical Transactions of the Royal Society of London A: Mathematical, Physical and Engineering Sciences **364**(1849), 3521-3537.
11. Sinclair G, Jordan P, Courtial J, Padgett M, Cooper J, Laczik ZJ (2004) Assembly of 3-dimensional structures using programmable holographic optical tweezers. Optics Express **12**(22), 5475-5480.
12. Roichman Y, Grier DG (2005) Holographic assembly of quasicrystalline photonic heterostructures. Optics express **13**(14), 5434-5439.
13. Čižmár T, Romero LD, Dholakia K, Andrews DL (2010) Multiple optical trapping and binding: new routes to self-assembly. Journal of Physics B: Atomic, Molecular and Optical Physics **43**(10), 102001.
14. Agarwal R, Ladavac K, Roichman Y, Yu G, Lieber CM, Grier DG (2005) Manipulation and assembly of nanowires with holographic optical traps. Optics Express **13**(22), 8906-8912.
15. Phillips DB, Grieve JA, Olof SN, Kocher SJ, Bowman R, Padgett MJ, Carberry DM (2011) Surface imaging using holographic optical tweezers. Nanotechnology **22**(28), 285503.
16. Brandt EH (2001) Acoustic physics: suspended by sound. Nature **413**, 474–475.
17. Bruus H (2012) Acoustofluidics 7: the acoustic radiation force on small particles. Lab Chip **12**, 1014–1021.
18. Lam KH et al. (2013) Ultrahigh frequency lensless ultrasonic transducers for acoustic tweezers application. Biotechnol Bioeng **110**, 881–886.
19. Lee J et al. (2009) Single beam acoustic trapping. Appl. Phys. Lett **95**, 073701.
20. Foresti D, Poulikakos D (2014) Acoustophoretic contactless elevation, orbital transport and spinning of matter in air. Phys. Rev. Lett **112**, 024301.
21. Courtney CR, Demore CE, Wu H, Grinenko A, Wilcox PD, Cochran S, Drinkwater BW (2014) Independent trapping and manipulation of microparticles using dexterous acoustic tweezers. Applied Physics Letters **104**(15), 154103.
22. Kang ST, Yeh CK (2010) Potential-well model in acoustic tweezers. IEEE Trans. Ultrason. Ferroelect. Freq. Control **57**, 1451–1459.
23. Li Y, Lee C, Chen R, Zhou Q, Shung KK (2014) A feasibility study of in vivo applications of single beam acoustic tweezers. Applied physics letters **105**(17), 173701.
24. Riaud A, Baudoin M, Matar OB, Becerra L, Thomas JL (2017) Selective manipulation of microscopic particles with precursor swirling rayleigh waves. Physical Review Applied **7**(2), 024007.
25. Laurell T, Petersson F, Nilsson A (2007) Chip integrated strategies for acoustic separation and manipulation of cells and particles. Chem. Soc. Rev. **36**, 492–506.
26. Ding X et al. (2012) On-chip manipulation of single microparticles, cells, and organisms using surface acoustic waves. Proc. Natl Acad. Sci. USA **109**, 11105–11109.
27. Whymark RR (1975) Acoustic field positioning for containerless processing. Ultrasonics **13**, 251–261.
28. Maxwell AD, Bailey M, Cunitz BW, Terzi M, Nikolaeva A, Tsysar S, Sapozhnikov OA (2016) Vortex beams and radiation torque for kidney stone management. The Journal of the Acoustical Society of America **139**(4), 2040-2040.
29. Hoshi T, Ochiai Y, Rekimoto J (2014) Three-dimensional noncontact manipulation by opposite ultrasonic phased arrays. Japanese Journal of Applied Physics **53**(7S), 07KE07.
30. Marzo A, Seah SA, Drinkwater BW, Sahoo DR, Long B, Subramanian S (2015) Holographic acoustic elements for manipulation of levitated objects. Nature communications **6**, 8661.
31. Prisbrey M, Raeymaekers B (2018) Ultrasound Noncontact Particle Manipulation of Three-dimensional Dynamic User-specified Patterns of Particles in Air. Physical Review Applied **10**(3), 034066.
32. Melde K, Mark AG, Qiu T, Fischer P (2016) Holograms for acoustics. Nature **537**(7621), 518.
33. Watanabe A, Hasegawa K, Abe Y (2018). Contactless Fluid Manipulation in Air: Droplet Coalescence and Active Mixing by Acoustic Levitation. Scientific reports **8**(1), 10221.
34. Inoue S, Mogami S, Ichiyama T, Noda A, Makino Y, Shinoda H (2017) Acoustic Macroscopic Rigid Body Levitation by Responsive Boundary Hologram. arXiv preprint arXiv:1708.05988.
35. Grier DG (2003) A revolution in optical manipulation. Nature **424**(6950), 810.
36. Melde K, Choi E, Wu Z, Palagi S, Qiu T, Fischer P (2018) Acoustic fabrication via the assembly and fusion of particles. Advanced Materials **30**(3), 1704507.
37. Baresch D, Thomas JL, Marchiano R (2016) Observation of a single-beam gradient force acoustical trap for elastic particles: acoustical tweezers. Physical review letters **116**(2), 024301.
38. Gerchberg RW, Saxton WO (1972) A practical algorithm for the determination of the phase from image and diffraction plane pictures . Optik **35**, 237.
39. Kim MG, Park J, Lim HG, Yoon S, Lee C, Chang JH, Shung KK (2017) Label-free analysis of the characteristics of a single cell trapped by acoustic tweezers. Scientific reports **7**(1), 14092.
40. Rayleigh L (1879) XXXI. Investigations in optics, with special reference to the spectroscope. The London, Edinburgh, and Dublin Philosophical Magazine and Journal of Science **8**(49), 261-274.
41. Hefner BT, Marston PL (1999) An acoustical helicoidal wave transducer with applications for the alignment of ultrasonic and underwater systems. The Journal of the Acoustical Society of America **106**(6), 3313-3316
42. Skeldon KD, Wilson C, Edgar M, Padgett MJ (2008) An acoustic spanner and its associated rotational Doppler shift. New Journal of Physics **10**(1), 013018.
43. Volke-Sepúlveda K, Santillán AO, Boullosa RR (2008) Transfer of angular momentum to matter from acoustical vortices in free space. Physical review letters **100**(2), 024302.
44. Marzo A, Caleap M, Drinkwater BW (2018) Acoustic Virtual Vortices with Tunable Orbital

Angular Momentum for Trapping of Mie Particles. Physical review letters **120**(4), 044301.
45. Foresti D, Poulikakos D (2014) Acoustophoretic contactless elevation, orbital transport and spinning of matter in air. Physical review letters **112**(2), 024301.
46. Franklin A, Marzo A, Malkin R, Drinkwater BW (2017) Three-dimensional ultrasonic trapping of micro-particles in water with a simple and compact two-element transducer. Applied Physic Letters **111**(9), 094101.
47. Cox L, Croxford A, Drinkwater BW, Marzo A (2018) Acoustic Lock: Position and orientation trapping of non-spherical sub-wavelength particles in mid-air using a single-axis acoustic levitator. Applied Physics Letters **113**(5), 054101.
48. Wu J (1991) Acoustical tweezers. The Journal of the Acoustical Society of America **89**(5), 2140-2143.
49. Grier DG, Roichman Y (2006) Holographic optical trapping. Applied optics **45**(5), 880-887.
50. Nyquist H (1928) Certain topics in telegraph transmission theory. Transactions of the American Institute of Electrical Engineers **47**(2), 617-644.
51. Marzo A, Corkett T, Drinkwater BW (2018) Ultraino: An Open Phased-Array System for Narrowband Airborne Ultrasound Transmission. IEEE transactions on ultrasonics, ferroelectrics, and frequency control **65**(1), 102-111
52. Hesseling C, Woerdemann M, Hermerschmidt A, Denz C (2011) Controlling ghost traps in holographic optical tweezers. Optics letters **36**(18), 3657-3659.
53. Airy GB (1835). On the diffraction of an object-glass with circular aperture. Transactions of the Cambridge Philosophical Society **5**, 283.
54. Waag RC, Fedewa RJ (2006) A ring transducer system for medical. IEEE transactions on ultrasonics, ferroelectrics, and frequency control **53**(10).
55. Wygant IO, Zhuang X, Yeh DT, Oralkan O, Ergun AS, Karaman M, Khuri-Yakub BT (2008) Integration of 2D CMUT arrays with front-end electronics for volumetric ultrasound imaging. IEEE transactions on ultrasonics, ferroelectrics, and frequency control **55**(2).
56. Smalley DE, Nygaard E, Squire K, Van Wagoner J, Rasmussen J, Gneiting S, ..., Costner K (2018) A photophoretic-trap volumetric display. Nature **553**(7689), 486.

Submission PDF